Research Article Vol. 41, No. 6 / June 2024 / Journal of the Optical Society of America B 1347

Journal of the Optical Society of America B

OPTICAL PHYSICS

Relative strengths of sum and difference frequency generation in perturbative high harmonic wave mixing

Zijuan Wei,[1] Mingdong Yan,[1] Fan Xia,[1] Ting Men,[1] Weiqi Tang,[1] Weiwei Yan,[1] Shiyuan Liu,[1,2,3] and Zhengyan Li[1,2,*]

[1]School of Optical and Electronic Information and Wuhan National Laboratory of Optoelectronics, Huazhong University of Science and Technology, Wuhan 430074, China
[2]Optics Valley Laboratory, Wuhan 430074, China
[3]School of Mechanical Engineering, Huazhong University of Science and Technology, Wuhan 430074, China
*zhengyanli@hust.edu.cn

Received 1 April 2024; accepted 6 May 2024; posted 9 May 2024; published 17 May 2024

High harmonic generation (HHG) modulated by a weak laser field allows the perturbative wave mixing process which involves sum and difference frequency generations (SFG and DFG). The relative strengths of SFG and DFG have been extensively discussed in the literature but are still ambiguous. Here we experimentally study the relative strengths between SFG and DFG channels by applying a frequency-offset second-harmonic perturbing laser field collinearly in a thin gaseous nonlinear medium. It shows that SFG is favored for low harmonic orders, but DFG dominates for high-energy photons, when only short trajectories of high harmonics are considered. A semi-classical model incorporating both modulations to the tunneling ionization and the electron propagation steps by the perturbing laser field for a train of attosecond pulses explains the experimental results.

https://doi.org/10.1364/JOSAB.525386

1. INTRODUCTION

High harmonic generation (HHG) driven by an intense laser pulse is an extremely nonlinear optical process involving three steps: electron tunneling ionization, free propagation in the laser field, and recombination with its parental ion [1,2]. Two laser pulses with different wavelengths are applied in "two-color" experiments [3–7], to improve the high harmonic conversion efficiency [8–10], to generate isolated attosecond pulses [11–13], or to probe ultrafast electron dynamics [14,15]. If one of these two laser pulses is significantly weaker than the other by 3–4 orders of magnitude in intensity, a high harmonic wave mixing process happens that new frequency components at $\Omega = n_1\omega_1 + n_2\omega_2$ are observed (ω_1 and ω_2 are the central frequencies of the driving and perturbing laser fields, respectively, and $n_1 > 0$ and n_2 are integers) [16].

The perturbative high harmonic wave mixing process has been applied to measure and control the spectral [17,18] or spatial [19–21] phase of attosecond pulses using a second-harmonic perturbing field. Such phase measurement or control strategies can be interpreted as an interferometer with two "arms" of different coherent, degenerate wave mixing channels, and the phase difference between these two arms is adjusted by tuning the time delay between the driving and perturbing laser fields. Such interpretation is successful based on the strong field approximation [22], except that it predicts the same strengths of degenerate SFG and DFG channels (the same Ω but opposite signs of n_2), contradicting experimental results in Ref. [16] that SFG is favored.

The relative strengths between SFG and DFG channels have been studied. For high harmonics generated by a 790 nm driving laser pulse and a collinear 500 nm perturbing laser field, the relative strength between the first-order SFG ($n_2 = 1$) and DFG ($n_2 = -1$) depends on the type of gaseous medium [6]. This observation is qualitatively explained that either the interference between quantum trajectories or the continuum state dressed by the perturbing laser field is responsible for the strength difference between SFG and DFG channels [6,23,24]. If the perturbing laser field wavelength is significantly larger than that of the driving field, a quasi-static perturbing field approximation is valid [25–27], predicting comparable SFG and DFG strengths in theory. When the macroscopic propagation effect of high harmonic generation is taken into account in a noncollinear perturbing geometry, the DFG channel is observed to be dominant to the SFG one in experiments [28], but a more recent study shows that SFG and DFG channels have similar strengths when the driving and perturbing fields have the same wavelengths [29].

In this paper, we have studied the perturbative high harmonic wave mixing process which is induced by a collinear, frequency-offset second-harmonic laser field. We choose such a perturbing laser wavelength for two reasons. First, previous experiments for high harmonic spectral or spatial phase measurement and control are closely related to the wave mixing process perturbed by a second-harmonic laser field. Second, in a collinear geometry, the slightly frequency-offset second-harmonic perturbing field allows the separation of SFG and DFG channels from the degenerate even harmonics without the macroscopic propagation effect. Our results show that the relative strengths between SFG and DFG channels are not only determined by their quantum phase difference during the second step of electron propagation but also affected by the perturbing field modulated ionization rate in the first step.

2. EXPERIMENTAL SETUPS AND RESULTS

The experimental setup is shown in Fig. 1(a). An 800 nm, 40 fs laser pulse is focused by a spherical mirror (300 mm focal length) to a 100-μm-thick gas jet, generating high harmonics which are measured by a spectrometer consisting of an incident slit, a flat-field extreme ultraviolet grating, and a microchannel plate detector. Limited by the spectrometer slit, only small-diverging short-trajectory components of high harmonic radiation are captured [30]. Although long trajectories in solid high harmonic generation may also contribute to small-divergence components [31], those we measured are only due to short trajectories because a positive atto-chirp is observed when a standard *in situ* measurement scheme is applied with a 400 nm perturbing field [17]. The perturbing field is generated by frequency-doubling the fundamental beam in a 3-mm-thick barium borate (BBO) crystal and combined with the driving laser beam collinearly with a dichroic mirror. The central wavelength of the perturbing field can be tuned from 390 to 415 nm with a narrow bandwidth of <3 nm by rotating the thick BBO crystal for a different phase-matching angle. Figure 1(b) shows the spectra of the perturbing laser centered at 411 nm and 396 nm. The perturbing laser intensity is 4 orders of magnitude lower than the driving one. The driving laser pulse energy is tuned to 0.38 mJ for argon gas medium and 0.80 mJ for neon with an adjustable neutral density filter.

Figure 2(a) shows high harmonic generation from argon [the driving laser intensity $I_1 = (1.78 \pm 0.08) \times 10^{14}$ W/cm^2, the perturbing and driving laser intensity ratio $I_2/I_1 \sim 10^{-4}$]

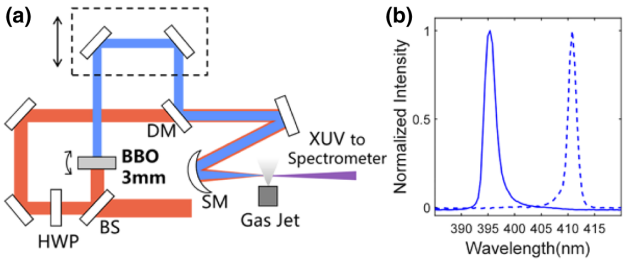

Fig. 1. (a) Schematic diagram of the experimental setup. BS for 50/50 beam splitter, HWP for half-wave plate, DM for dichroic mirror, and SM for spherical mirror. (b) The spectra of the perturbing laser field centered at 396 nm (solid line) and 411 nm (dashed line) are obtained by rotating the BBO crystal.

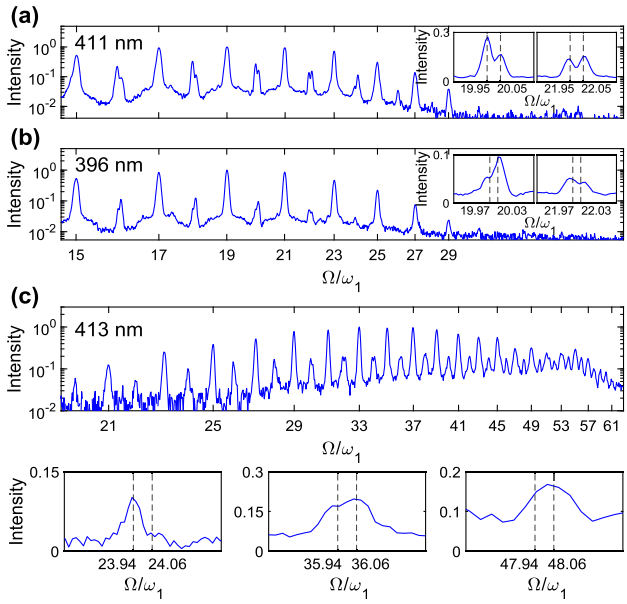

Fig. 2. High harmonic spectra from different gases with different perturbing laser wavelengths. (a) and (b) show high harmonic spectra in argon; the perturbative laser wavelengths are (a) 411 nm and (b) 396 nm. Insets show the zoomed-in spectra at $\Omega \sim 20\omega_1$ and $22\omega_1$. (c) High harmonic spectra from neon with perturbative laser wavelengths of 413 nm. Zoomed-in spectra at $\Omega \sim 24\omega_1$ (left), $36\omega_1$ (middle), and $48\omega_1$ (right) are shown in the bottom panels.

with a 411 nm perturbing laser field ($\omega_2 = 1.95\omega_1$). Besides odd-order harmonics, new wave mixing components are generated around even orders. For example, separated spectral peaks at $\Omega = 19.95\omega_1$ and $20.05\omega_1$ are observed around the 20th order [Fig. 2(a) inset, left panel], corresponding to SFG [$(n_1, n_2) = (18, +1)$] and DFG [$(n_1, n_2) = (22, -1)$] channels, respectively. For wave mixing components around 16, 18, $20\omega_1$, the SFG strengths are higher than the corresponding DFG ones. However, for that around 22 ω_1 [Fig. 2(a) inset, right panel], the DFG channel at 22.05 ω_1 is dominant to the SFG at $21.95\omega_1$. We then rotate the BBO crystal and tune the perturbing laser central wavelength to 396 nm ($\omega_2 = 2.03\omega_1$); wave mixing components are still observed [Fig. 2(b)]. Though it is different from the previous $\omega_2 < 2\omega_1$ case that high-frequency components around even harmonic orders are due to SFG and low-frequency ones are due to DFG, the experimental results that SFG is stronger than DFG for $\Omega \leq 20\omega_1$ and DFG is stronger than SFG for $\Omega \geq 22\omega_1$ are still valid [Fig. 2(b) inset]. The relative strengths between SFG and DFG are independent of the time delay between the driving and perturbing laser fields once they overlap, because SFG and DFG channels are separated in the spectra.

High harmonic wave mixing is also experimentally observed with a different gas medium of neon [$I_1 = (3.75 \pm 0.08) \times 10^{14}$ W/cm^2] [Fig. 2(c)], with the perturbing laser central wavelength at 413 nm ($\omega_2 = 1.94\omega_1$, $I_2/I_1 \sim 10^{-4}$). For low harmonic orders ($\Omega \leq 32\omega_1$), SFG components are more intense than DFG ones, for example, the SFG intensity at $\Omega = 23.94\omega_1 = 22\omega_1 + \omega_2$ is higher than DFG at $\Omega = 24.06\omega_1 = 26\omega_1 - \omega_2$ [Fig. 2(c), bottom left panel]. For

harmonic orders $\Omega \geq 36\omega_1$, DFG channels with larger photon energies are favored compared to SFG channels [Fig. 2(c), bottom middle panel]. Though SFG and DFG cannot be separated for higher-order harmonics (e.g., $\Omega \sim 48\omega_1$) due to their broader bandwidths and the resolution limit of the spectrometer, it is still observed that DFG is dominant because the peak of the merged wave mixing components shifts from $\Omega = 48\omega_1$ toward the high photon energy end.

When we discuss the relative significance of SFG and DFG channels, it is necessary to exclude the influence of the macroscopic propagation effect [23,28,29]. In our experiments with a loosely focused laser beam interacting with a short, tenuous gas medium (<200 μm) from a supersonic jet, the difference between the total phase accumulations in the medium for SFG and DFG channels around the same even harmonic order is less than 4 mrad. Thus, we take only the single-atom response into account in the following analysis.

3. THEORETICAL ANALYSIS

We next theoretically analyze the experimental results based on the strong field approximation [22]. The dipole moment emitting high harmonics in a time-varying laser field $\mathbf{E}(t) = \mathbf{E}_0 \cos(\omega_1 t)$ is

$$\mathbf{d}(t) = -i \int \mathrm{d}t_i \int \mathrm{d}\mathbf{k} \mathbf{b}^*(t) \left[\mathbf{E}(t_i) \cdot \mathbf{b}(t_i)\right] \times \exp[-iS(t, t_i, \mathbf{k})] + \text{c.c.}, \quad (1)$$

where $\mathbf{b}(t)$ is the bound-free transition dipole matrix element between the continuum Volkov state and the bound ground state, and $S(t, t_i, \mathbf{k}) = \frac{1}{2}\int_{t_i}^{t} [\mathbf{k} + \mathbf{A}(\tau)]^2 \mathrm{d}\tau + I_p(t - t_i)$ is the semi-classical action of the quantum trajectory with emission time t, ionization time t_i, and canonical momentum $\mathbf{k}$. Here I_p is the ionization potential of the gas medium, and $\mathbf{A}(t) = -\frac{\mathbf{E}_0}{\omega_1} \sin(\omega_1 t)$ is the vector potential of the total laser field including the driving and perturbing components. A saddle-point analysis scheme uniquely determines the dominant quantum trajectory contributing to the integral of $\mathbf{d}(t)$, corresponding to the stationary quantum phase saddle point with ionization time $t_i^{(s)}$ and canonical momentum $\mathbf{k}^{(s)}$ that satisfy $\nabla S(t, t_i^{(s)}, \mathbf{k}^{(s)}) = 0$. We first integrate over $\mathbf{k}$ around $\mathbf{k}^{(s)} = -(t - t_i)^{-1} \int_{t_i}^{t} \mathbf{A}(\tau)\mathrm{d}\tau$ and obtain a factor proportional to $|t - t_i|^{-3/2}$, which describes the quantum diffusion and is realistic because the singularity case ($t = t_i$) corresponds to zero ionization rate. To integrate over the ionization time t_i, we follow the strategy in Refs. [32,33] by introducing an imaginary part of the saddle ionization time, and the integration over its real part $t_i^{(s)}$ satisfying $\mathbf{A}(t_i^{(s)}) + \mathbf{k}^{(s)} = 0$ leads to another factor $a_i(t_i^{(s)}) = [\mathbf{E}(t_i^{(s)}) \cdot \mathbf{b}(t_i^{(s)})]|\mathbf{E}(t_i^{(s)})|^{-1/2} \exp[-\frac{(2I_p)^{3/2}}{3|\mathbf{E}(t_i^{(s)})|}]$ related to the ionization rate. The dipole moment is as follows (a brief derivation can be found in Appendix A):

$$\mathbf{d}(t) \propto \frac{\mathbf{b}^*(t)\left[\mathbf{E}(t_i^{(s)}) \cdot \mathbf{b}(t_i^{(s)})\right]}{|t - t_i^{(s)}|^{\frac{3}{2}} \sqrt{|\mathbf{E}(t_i^{(s)})|}} \exp\left(-\frac{(2I_p)^{\frac{3}{2}}}{3|\mathbf{E}(t_i^{(s)})|}\right) \times \exp[-iS(t, t_i^{(s)}, \mathbf{k}^{(s)})] + \text{c.c.} \quad (2)$$

If the perturbing laser field $\delta E(t) = \varepsilon E_0 \cos(\omega_2 t + \varphi)$ related to the perturbing field vector potential $\delta A(t)$ is applied ($\varepsilon \ll 1$ and the arbitrary phase delay φ is irrelevant), both the quantum phase $S(t, t_i^{(s)}, k^{(s)})$ and the dipole moment amplitude $\propto |t - t_i^{(s)}|^{-3/2} a_i(t_i^{(s)})$ are modulated. The quantum phase modulation can be calculated according to Ref. [17], i.e.,

$$\delta S\left(t, t_i^{(s)}, k^{(s)}\right) = \int_{t_i^{(s)}}^{t} \left[k^{(s)} + A(\tau) + \frac{I_p}{E(t_i^{(s)})\left(t - t_i^{(s)}\right)}\right] \times \delta A(\tau)\mathrm{d}\tau - \frac{I_p \delta A(t_i^{(s)})}{E(t_i^{(s)})}, \quad (3)$$

but extra terms $I_p[E(t_i^{(s)})(t - t_i^{(s)})]^{-1}$ and $I_p \delta A(t_i^{(s)}) E^{-1}(t_i^{(s)})$ are due to the saddle ionization time variation.

The amplitude modulation is

$$\delta\left[|t - t_i^{(s)}|^{-\frac{3}{2}} a_i(t_i^{(s)})\right] = \partial_{t_i^{(s)}}\left[|t - t_i^{(s)}|^{-\frac{3}{2}} a_i(t_i^{(s)})\right] \cdot \delta t_i^{(s)} + \left|t - t_i^{(s)}\right|^{-3/2} \partial_E a_i \left[\partial_{t_i^{(s)}} E(t_i^{(s)}) \cdot \delta t_i^{(s)} + \delta E(t_i^{(s)})\right], \quad (4)$$

with the first two terms due to the ionization time variation. The first term is $\sim \varepsilon |t - t_i^{(s)}|^{-3/2} a_i(t_i^{(s)})$, while the second and third terms are $\sim \varepsilon |t - t_i^{(s)}|^{-3/2} a_i(t_i^{(s)})(2I_p)^{3/2}|E(t_i^{(s)})|^{-1}$ much larger than the first term because the ponderomotive potential $U_p \sim E_0^2/\omega_1^2 \sim I_p \gg \omega_1$. So the perturbed dipole moment is as follows (a brief derivation can be found in Appendix B):

$$d_{\text{per}}(t) = d(t)\left\{1 + \frac{(2I_p)^{\frac{3}{2}}}{3\left|E(t_i^{(s)})\right| E(t_i^{(s)})}\left[\delta E(t_i^{(s)}) + \frac{\partial E(t_i^{(s)})}{\partial t_i^{(s)}} \delta t_i^{(s)}\right]\right\} \times \exp\left\{-i\int_{t_i^{(s)}}^{t}\left[k^{(s)} + A(\tau) + \frac{I_p}{E(t_i^{(s)})\left(t - t_i^{(s)}\right)}\right]\delta A(\tau)\mathrm{d}\tau + \frac{i I_p \delta A(t_i^{(s)})}{E(t_i^{(s)})}\right\} + \text{c.c.} \quad (5)$$

Now we define the effective emission time t' within a half of an optical cycle for the nth attosecond pulse, so $t' = t - nT_0/2$, where $T_0 = 2\pi/\omega_1$ and the driving field reaches its extremum at $t' = 0$. Then a Fourier transformation scheme applied to $d_{\text{per}}(n, t')$ with respect to the emission time t' for a long laser pulse yields the spectrum of the perturbed high harmonic generation is given by

$$
\begin{aligned}
&\tilde{d}_{\mathrm{per}}(\Omega)\\
&=\int e^{i\Omega\left(\frac{nT_0}{2}+t'\right)}d_{\mathrm{per}}(n,t')\mathrm{d}t'\\
&=\sum_n e^{i\Omega\frac{nT_0}{2}}(-1)^n\int e^{i\Omega t'}d^n_{\mathrm{per}}(t')\mathrm{d}t'\\
&=\sum_n e^{i(\Omega-\omega_1)\frac{nT_0}{2}}\int \mathrm{d}t' e^{i\Omega t'}\mathrm{d}(t')\\
&\times\left\{1+\frac{\varepsilon}{2}\left[u-\frac{\omega_2}{i}\left(t'-t_i^{(s)'}\right)v+v\right]e^{i\frac{nT_0}{2}(\omega_2-\omega_1)+i\varphi+i\omega_2 t_i^{(s)'}}\right.\\
&+\frac{\varepsilon}{2}\left[u+\frac{\omega_2}{i}\left(t'-t_i^{(s)'}\right)v+v\right]e^{-i\frac{nT_0}{2}(\omega_2-\omega_1)-i\varphi-i\omega_2 t_i^{(s)'}}\\
&\left.-\frac{\varepsilon}{2}ve^{i\frac{nT_0}{2}(\omega_2-\omega_1)+i\varphi+i\omega_2 t'}-\frac{\varepsilon}{2}ve^{-i\frac{nT_0}{2}(\omega_2-\omega_1)-i\varphi-i\omega_2 t'}\right\}\\
&\times\sum_{m_1=-\infty}^{\infty}J_{m_1}\left[\frac{\varepsilon E_0^2}{\omega_1\omega_2}\left|g\left(t'\right)\right|\right]e^{im_1\frac{nT_0}{2}(\omega_2-\omega_1)+im_1\varphi+im_1\arg[g(t')]}\\
&\times\sum_{m_2=-\infty}^{\infty}J_{m_2}\left[-\frac{\varepsilon I_p}{\omega_2\cos\left(\omega_1 t_i^{(s)'}\right)}\right]\\
&\times e^{im_2\frac{nT_0}{2}(\omega_2-\omega_1)+im_2\varphi+im_2\omega_2 t_i^{(s)'}}+\mathrm{c.c.},
\end{aligned}
\tag{6}
$$

where $u=\frac{(2I_p)^{\frac{3}{2}}}{3E_0\cos^2(\omega_1 t_i^{(s)'})}$, $v=\frac{-(2I_p)^{\frac{3}{2}}\omega_1\sin(\omega_1 t_i^{(s)'})}{3E_0\omega_2^2\cos^3(\omega_1 t_i^{(s)'})(t'-t_i^{(s)'})}$, $g=\int_{t_i^{(s)'}}^{t'}[\sin(\omega_1 t_i^{(s)'})-\sin(\omega_1\tau')+\frac{I_p\omega_1}{E_0^2\cos(\omega_1 t_i^{(s)'})(t'-t_i^{(s)'})}]e^{i\omega_2\tau'}\mathrm{d}\tau'$. And J_{m_1}, J_{m_2} are the Bessel functions of the first kind.

We only keep the first-order terms corresponding to wave mixing components for $|n_2|=1$ that (a brief derivation can be found in Appendix C)

$$
\begin{aligned}
\tilde{d}^{(1)}_{\mathrm{per}}(\Omega)\propto&\int \mathrm{d}t'^{e^{i\Omega(=n_1\omega_1-\omega_2)t'+i\varphi}}\mathrm{d}(t')\\
&\times\left\{\begin{array}{l}\left[u-\frac{\omega_2}{i}\left(t'-t_i^{(s)'}\right)v+v\right]e^{i\omega_2 t_i^{(s)'}}\\ -ve^{i\omega_2 t'}+\frac{E_0^2}{\omega_1\omega_2}g(t')-\frac{I_p e^{i\omega_2 t_i^{(s)'}}}{\omega_2\cos\left(\omega_1 t_i^{(s)'}\right)}\end{array}\right\}\\
&+\int \mathrm{d}t'^{e^{i\Omega(=n_1\omega_1+\omega_2)t'-i\varphi}}\mathrm{d}(t')\\
&\times\left\{\begin{array}{l}\left[u+\frac{\omega_2}{i}\left(t'-t_i^{(s)'}\right)v+v\right]e^{-i\omega_2 t_i^{(s)'}}\\ -ve^{-i\omega_2 t'}-\frac{E_0^2}{\omega_1\omega_2}g^*(t')+\frac{I_p e^{-i\omega_2 t_i^{(s)'}}}{\omega_2\cos\left(\omega_1 t_i^{(s)'}\right)}\end{array}\right\}+\mathrm{c.c.}
\end{aligned}
\tag{7}
$$

Equation (7) explicitly includes two terms corresponding to the SFG ($\Omega=n_1\omega_1+\omega_2$) and DFG ($\Omega=n_1\omega_1-\omega_2$) channels, and their relative intensities depend on the two terms of $[u-\frac{\omega_2}{i}(t'-t_i^{(s)'})v+v]e^{i\omega_2 t_i^{(s)'}}-ve^{i\omega_2 t'}$ and $\frac{E_0^2 g(t')}{\omega_1\omega_2}-\frac{I_p e^{i\omega_2 t_i^{(s)'}}}{\omega_2\cos(\omega_1 t_i^{(s)'})}$, which are due to perturbing field modulation of the electron ionization and the election propagation steps. Though Eq. (5) has also been extensively studied [17], only the quantum phase modulation in the second line describing the change of electron propagation trajectory (the second step in the three-step model) has been carefully considered. It diminishes the $[u-\frac{\omega_2}{i}(t'-t_i^{(s)'})v+v]e^{i\omega_2 t_i^{(s)'}}-ve^{i\omega_2 t'}$ terms in Eq. (7), leading to the conclusion that the SFG and DFG channels have the same intensities. However, if the perturbing-field-induced modulation on the electron ionization process (the first step in the three-step model) is taken into account, the opposite signs of the $\frac{\omega_2}{i}(t'-t_i^{(s)'})ve^{i\omega_2 t_i^{(s)'}}$, $\frac{E_0^2 g(t')}{\omega_1\omega_2}$, and $\frac{I_p e^{i\omega_2 t_i^{(s)'}}}{\omega_2\cos(\omega_1 t_i^{(s)'})}$ terms in Eq. (7) determine the relative strengths between the SFG and DFG channels.

We have calculated high harmonic generation with only short trajectory components based on Eq. (7) using parameters in our experiments. Figure 3(a) shows the intensities of SFG (open circles) and DFG (solid circles) components for high harmonic wave mixing in argon with the driving laser intensity of 1.85×10^{14} W/cm^2 and the perturbing field wavelengths are at 411 nm (blue) and 396 nm (red). It is clearly shown that SFG is dominant for low harmonic orders and DFG is more significant for high orders, and the transition happens at the harmonic order of 24, consistent with experimental results in Figs. 2(a) and 2(b) qualitatively. Figure 3(b) shows the calculation results of SFG and DFG in neon with the driving laser intensity 3.70×10^{14} W/cm^2 and the perturbing laser wavelengths at 413 nm. SFG components are stronger than corresponding DFG ones for low harmonic orders and vice versa. The boundary between these two regimes is around 36th harmonic orders, again explaining experimental observations in Fig. 2(c). In addition, the calculation results show that the signal intensity ratio $I_{\mathrm{DFG}}/I_{\mathrm{SFG}}$ is less than 0.35 below the 26th harmonic order, consistent with experimental results that corresponding DFG components are hardly measured in the experiment [Fig. 2(c), bottom left].

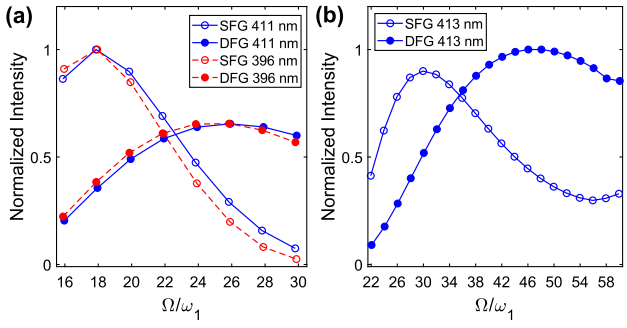

Fig. 3. Theoretical calculations of SFG (open circles) and DFG (solid dots) wave mixing components at even orders based on Eq. (7). (a) High harmonic spectra in argon with the perturbing laser wavelengths at 411 nm (blue, solid line) and 396 nm (red, dashed line). (b) High harmonic spectra in neon with the perturbing laser wavelengths at 413 nm.

We have also studied the effect of the driving laser intensity on the relative intensity between SFG and DFG channels. Figure 4(a) shows the measured intensity ratios between the DFG and SFG channels at different driving laser intensities ranging from $I_1 = (1.45 \pm 0.08) \times 10^{14}\,\mathrm{W/cm^2}$ to $(2.01 \pm 0.08) \times 10^{14}\,\mathrm{W/cm^2}$ while keeping the perturbing and driving laser intensity ratio constant ($I_2/I_1 \sim 10^{-4}$). As the driving laser intensity increases, the relative significance of SFG channels to corresponding DFG channels is enhanced for harmonic orders larger than 20, and the boundary between the SFG- and DFG-dominating regimes shifts to a higher harmonic order. For low harmonic orders smaller than 20, its dependence on the driving laser intensity is insignificant. We have compared the experimental results with theoretical calculations based on Eq. (7) as shown in Fig. 4(b), and their qualitative consistency confirms the role played by the ionization rate modulation induced by the perturbing laser field during the process of high harmonic wave mixing.

Not only short trajectory components of high harmonics are studied in experiments and theoretically analyzed, but the theoretical model in Eq. (7) is also applicable to high harmonics with both long and short trajectory components. Figures 5(a)–5(c) show the calculated DFG and SFG intensities taking both two trajectories into account in xenon ($I_1 = 1.22 \times 10^{14}\,\mathrm{W/cm^2}$), argon ($I_1 = 1.76 \times 10^{14}\,\mathrm{W/cm^2}$), and neon ($I_1 = 3.14 \times 10^{14}\,\mathrm{W/cm^2}$), and Figs. 5(d)–5(f) correspond to the situations where only the short trajectory is considered. When both long and short trajectories are considered, the DFG and SFG channels are comparable for xenon [Fig. 5(a)] and argon [Fig. 5(b)], while DFG channel is dominant for neon [Fig. 5(c)]. The behaviors are different from the case in that only short trajectories are considered [Figs. 5(d)–5(f)], because interference between short and long trajectories emissions has significant impact on the relative strengths between SFG and DFG channels. The long and short trajectory interference effect was proposed to explain previous experimental results [6,23,24], consistent with our calculation results in Figs. 5(a)–5(c).

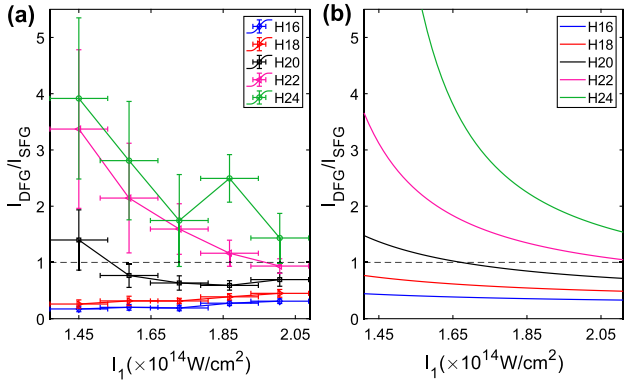

Fig. 4. Relative strengths between DFG and SFG channels at different driving laser intensities. (a) Measured $I_{\mathrm{DFG}}/I_{\mathrm{SFG}}$ of Ω close to 16, 18, 20, 22, 24 ω_1 as a function of the driving laser intensity. (b) Calculated results based on Eq. (7) for different driving laser intensities, as a comparison to experiments.

4. CONCLUSION

In summary, we have experimentally and theoretically studied the relative strengths between SFG and DFG channels in the process of perturbative high harmonic wave mixing. The difference between SFG and DFG intensities and its dependence on the harmonic order, the driving laser intensity, and so on suggests that it is insufficient to only consider the quantum phase modulation by the perturbing laser field within the second electron propagation step of the three-step model. Instead, the ionization rate changes due to the perturbing laser field during the first photoionization step should be considered to explain our experimental results of high harmonic wave mixing. This new insight into the high harmonic wave mixing process

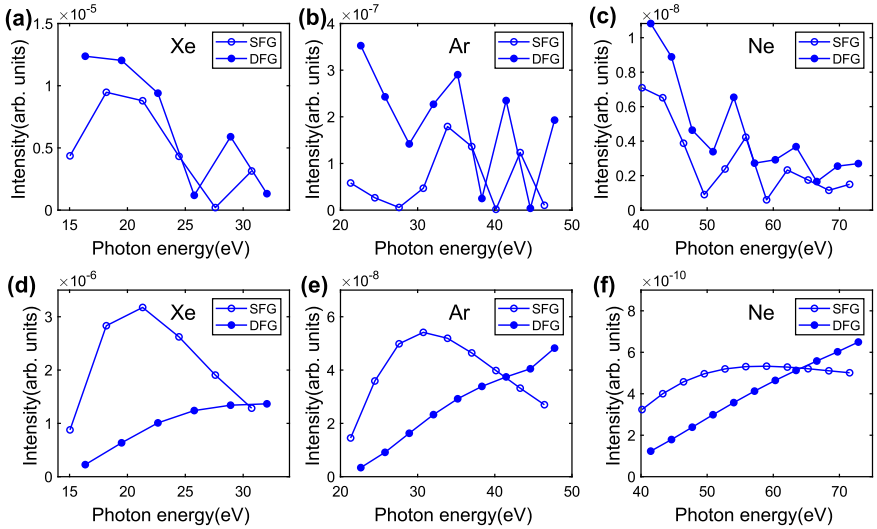

Fig. 5. Theoretical calculations of SFG (open circles) and DFG (solid dots) intensities generated by the 790 nm driving laser field and 500 nm perturbing laser field. The top row shows the results considering both long and short trajectories in (a) xenon, (b) argon, and (c) neon, while in the bottom row (d)–(f) only the short trajectory is considered in the three gases, respectively. The calculation parameters are similar to the experiments in Ref. [6].

not only enables one to spatiotemporally measure attosecond pulses with a more complete theoretical model [17], but also defines the working conditions of wavefront control for extreme ultraviolet high harmonic radiations [19,34].

APPENDIX A: SOLVING THE INTEGRAL OF THE DIPOLE MOMENT

Assuming that $\mathbf{d}(t)$ is a slowly changing function, we can use the saddle point analysis [32,33] to find the stationary phase points that contribute the most to solve this double integral.

The stationary phase point $\mathbf{k}^{(s)}$ satisfies $\mathbf{k}^{(s)}(t,t_i) = -\frac{1}{(t-t_i)}\int_{t_i}^{t}\mathbf{A}(\tau)\mathrm{d}\tau$. And the second derivative of $S(t,t_i,\mathbf{k})$ to $\mathbf{k}$ is $\frac{\partial^2 S(t,t_i,\mathbf{k})}{\partial \mathbf{k}^2}|_{\mathbf{k}^{(s)}} = \int_{t_i}^{t}\mathrm{d}\tau = t - t_i$. The stationary phase evaluation around $\mathbf{k}^{(s)}$ gives

$$\mathbf{d}(t) = -ie^{\frac{i3\pi}{4}}\int_{t_0}^{t}\mathrm{d}t_i\left(\frac{2\pi}{|t-t_i|}\right)^{\frac{3}{2}}\mathbf{b}^*(t)\left[\mathbf{E}(t_i)\cdot\mathbf{b}(t_i)\right] \times \exp\left[-iS\left(t,t_i,\mathbf{k}^{(s)}\right)\right] + \text{c.c.} \tag{A1}$$

The saddle points for t_i satisfy the equation $\frac{\partial S(t,t_i,\mathbf{k}^{(s)})}{\partial t_i} = -\frac{1}{2}[\mathbf{k}^{(s)} + \mathbf{A}(t_i)]^2 - I_p = 0$. Since the ionization potential I_p is positive, the solutions lead to complex ionization time $t_i^{(sc)} = t_i^{(s)} + \Delta$. The real part $t_i^{(s)}$ has the real physical meaning of the continuum electron birth time, and we perform the integration of Eq. (A1) around $t_i^{(s)}$, which satisfies

$$\mathbf{k}^{(s)} + \mathbf{A}(t_i^{(s)}) = 0. \tag{A2}$$

We expand $S(t,t_i,\mathbf{k}^{(s)})$ in a Taylor series around $t_i^{(s)}$ that $S(t,t_i,\mathbf{k}^{(s)}) = S(t,t_i^{(s)},\mathbf{k}^{(s)}) - I_p(t_i - t_i^{(s)}) - \frac{1}{6}|\mathbf{E}(t_i^{(s)})|^2 (t_i - t_i^{(s)})^3$. And the integration of Eq. (A1) now is

$$\mathbf{d}(t) = -ie^{\frac{i3\pi}{4}}\left(\frac{2\pi}{\left|t-t_i^{(s)}\right|}\right)^{\frac{3}{2}}\exp\left[-iS\left(t,t_i^{(s)},\mathbf{k}^{(s)}\right)\right]\mathbf{b}^*(t) \times\left[\mathbf{E}(t_i^{(s)})\cdot\mathbf{b}(t_i^{(s)})\right]\frac{1}{2\pi}\left[\frac{2}{I_p\left|\mathbf{E}(t_i^{(s)})\right|^2}\right]^{\frac{1}{4}} \times\exp\left[-\frac{(2I_p)^{\frac{3}{2}}}{3\left|\mathbf{E}(t_i^{(s)})\right|}\right] + \text{c.c.}, \tag{A3}$$

where the second line uses an asymptotic formula of $\int_{-\infty}^{\infty}\mathrm{d}t_i\, e^{i[I_p(t_i-t_i^{(s)})+\frac{1}{6}|\mathbf{E}(t_i^{(s)})|^2(t_i-t_i^{(s)})^3]} = \frac{2^{1/3}}{|\mathbf{E}(t_i^{(s)})|^{2/3}}\mathrm{Ai}\left(\frac{2^{1/3}I_p}{|\mathbf{E}(t_i^{(s)})|^{2/3}}\right)$, where Ai(z) is the Airy function.

The dipole moment finally is written as Eq. (2).

APPENDIX B: THE PERTURBED DIPOLE MOMENT

Recall the perturbing field introduced of $\delta\mathbf{E}(t) = \varepsilon E_0\cos(\omega_2 t+\varphi)\hat{\mathbf{x}}$, and the vector potential is $\delta\mathbf{A}(\mathrm{t}) = -\frac{\varepsilon E_0}{\omega_2}\sin(\omega_2 t+\varphi)\hat{\mathbf{x}}$. Assuming the fields are polarized along $\hat{\mathbf{x}}$ and omit vector notation because all vector quantities will be parallel to $\hat{\mathbf{x}}$.

From Appendix A there is $A(t_i^{(s)}) = \frac{1}{(t-t_i^{(s)})}\int_{t_i^{(s)}}^{t}A(\tau)\mathrm{d}\tau$ according to $k^{(s)} = -\frac{1}{(t-t_i^{(s)})}\int_{t_i^{(s)}}^{t}\mathrm{A}(\tau)\mathrm{d}\tau$ and $k^{(s)} + A(t_i^{(s)}) = 0$. Then we have

$$\delta A(t_i^{(s)})(t-t_i^{(s)}) + \left[\frac{\partial A(t_i^{(s)})}{\partial t_i^{(s)}}(t-t_i^{(s)}) - A(t_i^{(s)})\right]\delta t_i^{(s)} = \int_{t_i^{(s)}}^{t}\delta A(\tau)\mathrm{d}\tau - A(t_i^{(s)})\delta t_i^{(s)}. \tag{B1}$$

And the variation of the ionization time due to the perturbing laser field is

$$\delta t_i^{(s)} = \frac{\int_{t_i^{(s)}}^{t}\left[\delta A(t_i^{(s)}) - \delta A(\tau)\right]\mathrm{d}\tau}{E(t_i^{(s)})\left(t-t_i^{(s)}\right)}. \tag{B2}$$

We estimate the amount of the ionization time variation for observable high harmonics where the continuum electrons are ionized when the driving laser field reaches its maxima and the acceleration time $t - t_i^{(s)}$ is finite, so $|\delta t_i^{(s)}| \sim \frac{\varepsilon}{\omega_2}$.

Thus, the first term of Eq. (4) $\sim \varepsilon|t-t_i^{(s)}|^{-3/2}a_i(t_i^{(s)})$ is much smaller than the second and the third terms as mentioned in Section 3, which is negligible. The amplitude modulation is

$$\delta\left[\left|t-t_i^{(s)}\right|^{-\frac{3}{2}}a_i(t_i^{(s)})\right] \approx \left|t-t_i^{(s)}\right|^{-\frac{3}{2}}a_i(t_i^{(s)})\frac{(2I_p)^{\frac{3}{2}}}{3\left|E(t_i^{(s)})\right|} \times\left[\frac{\delta E(t_i^{(s)})}{E(t_i^{(s)})} + \frac{\delta t_i^{(s)}}{E(t_i^{(s)})}\frac{\partial E(t_i^{(s)})}{\partial t_i^{(s)}}\right]. \tag{B3}$$

By incorporating both the amplitude modulation of Eq. (B3) and quantum phase modulations of Eq. (3) into account, the dipole momentum in the presence of the perturbing field can be expressed as Eq. (5).

APPENDIX C: THE PERTURBED DIPOLE SPECTRUM

The nth perturbed dipole moment of the attosecond pulse trains is

$$d^{n}_{\mathrm{per}}(t') = (-1)^{n} d(t') \left(1 + \frac{\varepsilon (2I_p)^{\frac{3}{2}}}{3E_0 \cos^2\left(\omega_1 t_i^{(s)'}\right)} \cos\left[\frac{nT_0}{2}(\omega_2 - \omega_1) + \omega_2 t_i^{(s)'} + \varphi \right] \right.$$
$$+ \frac{\varepsilon (2I_p)^{\frac{3}{2}} \left[-\omega_1 \sin\left(\omega_1 t_i^{(s)'}\right) \right]}{3E_0 \cos^2\left(\omega_1 t_i^{(s)'}\right)} \left\{ \frac{-\omega_2 \sin\left[\frac{nT_0}{2}(\omega_2 - \omega_1) + \omega_2 t_i^{(s)'} + \varphi \right] \left(t' - t_i^{(s)'} \right)}{\omega_2^2 \cos\left(\omega_1 t_i^{(s)'}\right) \left(t' - t_i^{(s)'} \right)} \right.$$
$$\left. \left. + \frac{\cos\left[\frac{nT_0}{2}(\omega_2 - \omega_1) + \omega_2 t_i^{(s)'} + \varphi \right] - \cos\left[\frac{nT_0}{2}(\omega_2 - \omega_1) + \omega_2 t' + \varphi \right]}{\omega_2^2 \cos\left(\omega_1 t_i^{(s)'}\right) \left(t' - t_i^{(s)'} \right)} \right\} \right)$$
$$\times \exp\left\{ i \int_{t_i^{(s)'}}^{t'} \frac{\varepsilon E_0^2}{\omega_1 \omega_2} \left[\sin\left(\omega_1 t_i^{(s)'}\right) - \sin(\omega_1 \tau') + \frac{I_p \omega_1}{E_0^2 \cos\left(\omega_1 t_i^{(s)'}\right) \left(t' - t_i^{(s)'} \right)} \right] \right.$$
$$\left. \times \sin\left[\frac{nT_0}{2}(\omega_2 - \omega_1) + \omega_2 \tau' + \varphi \right] \mathrm{d}\tau' - i \frac{\varepsilon I_p \sin\left[\frac{nT_0}{2}(\omega_2 - \omega_1) + \omega_2 t_i^{(s)'} + \varphi \right]}{\omega_2 \cos\left(\omega_1 t_i^{(s)'}\right)} \right\} + \mathrm{c.c.}, \tag{B4}$$

where $(-1)^n \cos(\omega_2 \frac{nT_0}{2}) = \cos(\frac{nT_0}{2}\omega_2 - \frac{nT_0}{2}\omega_1)$.

Defining the u, v, and g as mentioned in Section 3, the HHG spectrum is then given by a Fourier transform as Eq. (6).

For the zeroth-order approximation (m_1, $m_2 = 0$) of Eq. (6), the dipole spectrum corresponds to high harmonic generation without the perturbing field, and there is only odd-order harmonics of the driving laser field:

$$\tilde{d}^{(0)}_{\mathrm{per}}(\Omega) = \sum_n e^{i(\Omega - \omega_1)\frac{nT_0}{2}} \int e^{i\Omega dt'} \mathrm{d}(t') J_0 \left[\frac{\varepsilon E_0^2}{\omega_1 \omega_2} |g(t')| \right] J_0 \left[-\frac{\varepsilon I_p}{\omega_2 \cos\left(\omega_1 t_i^{(s)'}\right)} \right] \mathrm{d}t' + \mathrm{c.c.}$$
$$= \delta\left[\Omega - (2x+1)\omega_1\right] \int e^{i\Omega t'} d(t') \mathrm{d}t' + \mathrm{c.c.}, \tag{B5}$$

where x is a positive integer.

For the first-order approximation, the spectrum of the dipole momentum is expressed as

$$\tilde{d}^{(1)}_{\mathrm{per}}(\Omega) = \sum_n e^{i(\Omega - \omega_1)\frac{nT_0}{2}} \int \mathrm{d}t' e^{i\Omega t'} \mathrm{d}(t') \left(\left\{ \frac{\varepsilon}{2} \left[u - \frac{\omega_2}{i} \left(t' - t_i^{(s)'} \right) v + v \right] e^{i\frac{nT_0}{2}(\omega_2 - \omega_1) + i\varphi + i\omega_2 t_i^{(s)'}} \right. \right.$$
$$+ \frac{\varepsilon}{2} \left[u + \frac{\omega_2}{i} \left(t' - t_i^{(s)'} \right) v + v \right] e^{-i\frac{nT_0}{2}(\omega_2 - \omega_1) - i\varphi - i\omega_2 t_i^{(s)'}} - \frac{\varepsilon}{2} v e^{i\frac{nT_0}{2}(\omega_2 - \omega_1) + i\varphi + i\omega_2 t'} \left. - \frac{\varepsilon}{2} v e^{-i\frac{nT_0}{2}(\omega_2 - \omega_1) - i\varphi - i\omega_2 t'} \right\}$$
$$+ J_1 \left[\frac{\varepsilon E_0^2}{\omega_1 \omega_2} |g(t')| \right] e^{i\frac{nT_0}{2}(\omega_2 - \omega_1) + i\varphi + i \arg[g(t')]} + J_{-1} \left[\frac{\varepsilon E_0^2}{\omega_1 \omega_2} |g(t')| \right] e^{-i\frac{nT_0}{2}(\omega_2 - \omega_1) - i\varphi - i \arg[g(t')]}$$
$$\left. + J_1 \left[-\frac{\varepsilon I_p}{\omega_2 \cos\left(\omega_1 t_i^{(s)'}\right)} \right] e^{i\frac{nT_0}{2}(\omega_2 - \omega_1) + i\varphi + i\omega_2 t_i^{(s)'}} + J_{-1} \left[-\frac{\varepsilon I_p}{\omega_2 \cos\left(\omega_1 t_i^{(s)'}\right)} \right] e^{-i\frac{nT_0}{2}(\omega_2 - \omega_1) - i\varphi - i\omega_2 t_i^{(s)'}} \right) + \mathrm{c.c.}, \tag{B6}$$

where $\lim_{x \to 0} J_1(x) \to \frac{1}{2}x$. The amplitude and phase terms can be rearranged according to the exponential terms.

The spectrum of the first-order perturbed dipole momentum is finally given by Eq. (7).

Funding. National Natural Science Foundation of China (12275099, 52130504); Basic and Applied Basic Research Foundation of Guangdong Province (2019B030302003); Innovation Project of Optics Valley Laboratory (OVL2021ZD001).

Disclosures. The authors declare no conflicts of interest.

Data availability. Data underlying the results presented in this paper are not publicly available at this time but may be obtained from the authors upon reasonable request.

REFERENCES

1. P. B. Corkum and F. Krausz, "Attosecond science," Nat. Phys. **3**, 381–387 (2007).
2. P. B. Corkum, "Plasma perspective on strong field multiphoton ionization," Phys. Rev. Lett. **71**, 1994–1997 (1993).
3. M. D. Perry and J. K. Crane, "High-order harmonic emission from mixed fields," Phys. Rev. A **48**, R4051–R4054 (1993).
4. H. Eichmann, S. Meyer, K. Riepl, *et al.*, "Generation of short-pulse tunable XUV radiation by high-order frequency mixing," Phys. Rev. A **50**, R2834–R2836 (1994).
5. S. Watanabe, K. Kondo, Y. Nabekawa, *et al.*, "Two-color phase control in tunneling ionization and harmonic generation by a strong laser field and its third harmonic," Phys. Rev. Lett. **73**, 2692–2695 (1994).
6. M. B. Gaarde, P. Antoine, A. Persson, *et al.*, "High-order tunable sum and difference frequency mixing in the XUV region," J. Phys. B **29**, L163–L168 (1996).
7. Y. Oguchi, S. Minemoto, and H. Sakai, "Dependence of the generation efficiency of high-order sum and difference frequencies in the extreme ultraviolet region on the wavelength of an added tunable laser field," J. Phys. Soc. Jpn. **80**, 014301 (2011).
8. C. Jin, G. Wang, H. Wei, *et al.*, "Waveforms for optimal sub-keV high-order harmonics with synthesized two- or three-colour laser fields," Nat. Commun. **5**, 4003 (2014).
9. B. D. Bruner, M. Krüger, O. Pedatzur, *et al.*, "Robust enhancement of high harmonic generation via attosecond control of ionization," Opt. Express **26**, 9310–9322 (2018).
10. M. A. Khokhlova and V. V. Strelkov, "Highly efficient XUV generation via high-order frequency mixing," New J. Phys. **22**, 093030 (2020).
11. P. Lan, P. Lu, W. Cao, *et al.*, "Isolated sub-100-as pulse generation via controlling electron dynamics," Phys. Rev. A **76**, 011402 (2007).
12. T. Shao, G. Zhao, B. Wen, *et al.*, "Theoretical exploration of laser-parameter effects on the generation of an isolated attosecond pulse from two-color high-order harmonic generation," Phys. Rev. A **82**, 063838 (2010).
13. E. J. Takahashi, P. Lan, O. D. Mücke, *et al.*, "Infrared two-color multicycle laser field synthesis for generating an intense attosecond pulse," Phys. Rev. Lett. **104**, 233901 (2010).
14. H. J. Wörner, J. B. Bertrand, B. Fabre, *et al.*, "Conical intersection dynamics in NO_2 probed by homodyne high-harmonic spectroscopy," Science **334**, 208–212 (2011).
15. G. Porat, G. Alon, S. Rozen, *et al.*, "Attosecond time-resolved photoelectron holography," Nat. Commun. **9**, 2805 (2018).
16. J. B. Bertrand, H. J. Wörner, H. C. Bandulet, *et al.*, "Ultrahigh-order wave mixing in noncollinear high harmonic generation," Phys. Rev. Lett. **106**, 023001 (2011).
17. N. Dudovich, O. Smirnova, J. Levesque, *et al.*, "Measuring and controlling the birth of attosecond XUV pulses," Nat. Phys. **2**, 781–786 (2006).
18. D. H. Ko, G. G. Brown, C. Zhang, *et al.*, "Near-field imaging of dipole emission modulated by an optical grating," Optica **8**, 1632–1637 (2021).
19. Z. Li, G. Brown, D. H. Ko, *et al.*, "Perturbative high harmonic wave front control," Phys. Rev. Lett. **118**, 033905 (2017).
20. F. Kong, C. Zhang, F. Bouchard, *et al.*, "Controlling the orbital angular momentum of high harmonic vortices," Nat. Commun. **8**, 14970 (2017).
21. K. T. Kim, C. Zhang, A. D. Shiner, *et al.*, "Manipulation of quantum paths for space–time characterization of attosecond pulses," Nat. Phys. **9**, 159–163 (2013).
22. M. Lewenstein, P. Balcou, M. Y. Ivanov, *et al.*, "Theory of high-harmonic generation by low-frequency laser fields," Phys. Rev. A **49**, 2117–2132 (1994).
23. P. Balcou, A. S. Dederichs, M. B. Gaarde, *et al.*, "Quantum-path analysis and phase matching of high-order harmonic generation and high-order frequency mixing processes in strong laser fields," J. Phys. B **32**, 2973–2989 (1999).
24. M. B. Gaarde, A. L'Huillier, and M. Lewenstein, "Theory of high-order sum and difference frequency mixing in a strong bichromatic laser field," Phys. Rev. A **54**, 4236–4248 (1996).
25. V. V. Strelkov, "High-order optical processes in intense laser field: towards nonperturbative nonlinear optics," Phys. Rev. A **93**, 053812 (2016).
26. F. V. Ignatovich, V. T. Platonenko, and V. V. Strelkov, "High-order harmonic generation by bichromatic field," Proc. SPIE **3735**, 215–224 (1999).
27. V. A. Birulia, M. A. Khokhlova, and V. V. Strelkov, "Generation of attosecond pulses with a controllable carrier-envelope phase via high-order frequency mixing," Phys. Rev. A **106**, 023514 (2022).
28. C. M. Heyl, P. Rudawski, F. Brizuela, *et al.*, "Macroscopic effects in noncollinear high-order harmonic generation," Phys. Rev. Lett. **112**, 143902 (2014).
29. C. Chappuis, D. Bresteau, T. Auguste, *et al.*, "High-order harmonic generation in an active grating," Phys. Rev. A **99**, 033806 (2019).
30. M. B. Gaarde, F. Salin, E. Constant, *et al.*, "Spatiotemporal separation of high harmonic radiation into two quantum path components," Phys. Rev. A **59**, 1367–1373 (1999).
31. Y. Wang, T. Shao, X. Li, *et al.*, "Trajectory-controlled high-order harmonic generation in ZnO crystals," Opt. Express **31**, 3379–3389 (2023).
32. C. J. Joachain, N. J. Kylstra, and R. M. Potvliege, *Atoms in Intense Laser Fields* (Cambridge University, 2012).
33. M. Y. Ivanov, T. Brabec, and N. Burnett, "Coulomb corrections and polarization effects in high-intensity high-harmonic emission," Phys. Rev. A **54**, 742–745 (1996).
34. Z. Li, F. Kong, G. Brown, *et al.*, "Perturbing laser field dependent high harmonic phase modulations," J. Phys. B **51**, 125601 (2018).